Comparison of optical and capacitive Dew Point Detection using COTS Components

Malte Nilges, David Riehl, Klaus Hofmann and Ferdinand Keil
Integrated Electronic Systems Lab, Technische Universität Darmstadt, Germany
Malte.Nilges@gmail.com, Ferdinand.Keil@ies.tu-darmstadt.de, Klaus.Hofmann@ies.tu-darmstadt.de

***Abstract*—This works presents a dew point temperature sensor employing parallel capacitive and optical readout of a chilled electroless nickel immersion gold (ENIG) surface. The use of commercial off the shelf (COTS) components and simple mechanical construction leads to a reproducible and cost-effective sensor system, which is put to test using saturated salt solutions in order to give a comprehensible comparison of capacitive and optical sensing methods. A multitude of sensors was put to test, including four temperature sensor models, two proximity sensors and an interdigital electrodes (IDE) capacitor.**

***Index Terms*—humidity, dew point, temperature sensor, cots, capacitance measurement, deliquescence**

I. Introduction

Dew point hygrometers are crucial for accurately measuring atmospheric moisture in various industrial and scientific applications, such as meteorology and semiconductor manufacturing. Compared to other measurement principles that can provide high temperature ranges of several hundred degrees celsius, accuracies in the millidegree range and adaptability to different gas mixtures [1]. Most research in these devices has been performed in optical methods, which detect the condensation on chilled mirrors through changes in light intensity caused by scattering or absorption [1]–[3]. While recent works involve new and precise techniques for dew point detection, such as a quartz oscillator [illegible] or a photonic resonator [5], these methods require manufacturing of custom sensors, leading to high cost in case of low volume production. This paper examines and compares [illegible] of optical and capacitive measurement methods for enabling low-cost dew point hygrometers.

II. Examination of Temperature Sensors

The temperature readout is a critical component of the sensor system, requiring high accuracy and fast response times as an error of 0.1 K can yield a deviation in relative humidity (RH) of up to 1 %. An early test evaluated multiple temperature sensors to identify suitable candidates for the platform. The test used a Fluke 561[illegible] platinum resistance thermometer (PRT), a Fluke 7320 calibration bath for temperature control and a Keysight 3458A multimeter. For a measurement duration of 60 s for each target temperature, the temperature sensors were read every 200 ms using a microcontroller and the reference temperature was determined every 2 s using a 4-wire resistance measurement of the PRT and its ITS-90 calibration coefficients. Based on the last recalibration cycle of approximately 3 years, the accuracy of the multimeter

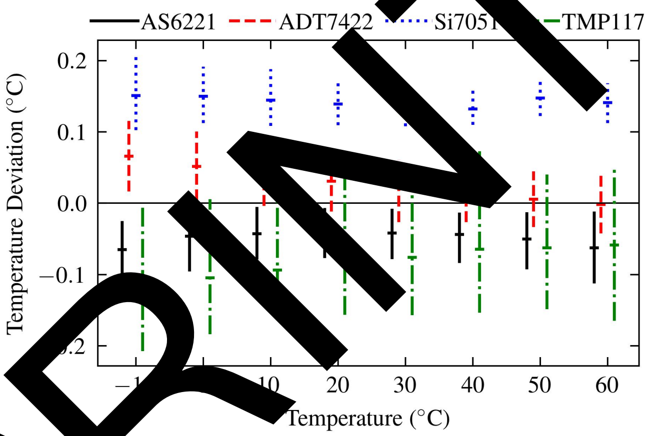

Fig. 1: Average, minimum and maximum temperature deviation of four devices of each temperature sensor model compared to the PRT.

can be assumed to be ±5 mK for the respective resistance measurement range of 100 kΩ and that of the PRT to be ±19 mK. Four different types of temperature sensors were put to test: AMS AS6221, Silicon Labs Si7051, Analog Devices ADT7422 and TI TMP117; of each type four devices on a single [illegible] mm × 4[illegible] mm printed circuit board (PCB). The test temperatures ranged from −10 °C to 60 °C in steps of 10 °C. Figure 1 shows the the average, minimum and maximum deviations in relation to the PRT reference, which itself deviates less than [illegible] mK during the complete measurement cycle. The results show that only the ADT7422 and AS6221 sensors were able to consistently measure the temperature within their respective specifications of 0.1 K and 0.09 K, with only few measurements exceeding the specification. The Si7051 devices had a consistent offset of around +0.15 K, leading to all measured devices being outside specification. The TMP117 devices were on average within specification, yet yielded most inconsistent temperature measurements, which may deviate around 0.2 K across timepoints and devices.

III. Methods

A. Hardware

The sensor platform is divided into two primary components: the base board and the mirror board. The base board integrates a cluster of proximity sensors, specifically the Vishay VCNL36825T, which utilizes a vertical cavity surface emitting laser with a narrow emission beam, and the Vishay VCNL4040, which employs an infrared light emitting diode (LED) with a broader emission beam.

The mirror board is designed as a flexible printed circuit (FPC) to minimize thermal resistance. It features an ENIG-coated copper surface which hosts an array of four Osram AS6221 temperature sensors. The surface is subdivided into one continuous part acting as a mirror surface for the proximity sensors and one interdigitated part acting as an IDE capacitor. A trace heater on the backside of the surface and a thermoelectric cooler mounted on top provide uniform and rapid temperature adjustments. For the capacitor readout, a relaxation oscillator using a single TI SN74LVC1G14 inverting Schmitt trigger is employed, which charges and discharges the capacitor. Its switching frequency depends on the capacitance, giving a direct measure of dew.

B. Software

The control software was written for the STM32 microcontroller platform, involving the set-up of thresholds for dew point presence based on initial sensor readings and thereafter the execution of multiple cooling and reheating cycles. The first cycle determines a dew point temperature window based on the initial thresholds using a fast cool down in order to avoid lenghty and inefficient cooling. Subsequent cycles work within this window and decrease the cool down speed in order to achieve higher resolution in temperature readout. Within every cycle, cooling and heating of the copper surface is regulated by a proportional-integral-derivative (PID) controller at a frequency of 5 Hz using the average temperature readings of the four sensors. The temperature, frequency and proximity readings are transferred to a host computer.

For the following data analysis, the system employs the use of smoothing splines as a regression technique [6], [illegible]. The splines use a minimal number of piecewise connected polynomials (B-splines) of nth degree to fit the resulting curve to the measurement data adhering to a [illegible] constraint that was determined empirically for the measurement data. This allows for a reduction of high frequency noise while offering a low amount of smoothing and delay in case of step changes in measurement data as compared to finite impulse response (FIR) filters using fixed window functions.

C. Testing Environment

In order to provide accurate measurements, a setup with salt solutions inside a properly sealed container was chosen to achieve a fixed-point humidity control. Four saturated salt solutions were used in a ventilated system for lowering the saturation vapour pressure as displayed in Table I. The values for the vapour pressures have been extensively researched and provide reliable assumptions about the reference humidity in the test setup [8]. Temperatures have been settled to an accuracy of $\pm 0.1\,\mathrm{K}$ and the ventilation was performed for at least three hours in order to achieve constant humidity.

TABLE I: Equilibrium Relative Humidities [8] and Measurement Errors of the Control Substances

Substance	T (°C)	RH (Δ) (%)	Measured ΔRH (%) IDE	OPT1	OPT2
$MgCl_2$	10 *	33.47 (±0.24)	-0.94	+0.06	+0.42
	25 *	32.78 (±0.16)	+0.61	-0.57	+0.36
	40 *	31.60 (±0.13)	-0.66	-0.87	-0.23
$Mg(NO_3)_2$ * $6H_2O$	10 *	57.36 (±0.33)	+0.07	+0.11	+0.11
	25	52.89 (±0.22)	+1.37	[illegible]1.68	+0.33
	40	48.42 (±0.37)	+3.29	-1.46	+8.68
NaCl	10	75.67 (±0.22)	[illegible]	+1.04	+3.62
	25	75.29 (±0.12)	[illegible]1.10	-3.02	+1.38
	40	74.68 (±0.13)	+4.44	[illegible].48	-1.48
K_2SO_4	10	98.18 (±0.[illegible])	+4.18	+1.[illegible]	+1.08
	25	97.59 (±0.53)	-0.75	-4.00	-1.27
	40	96.71 (±0.38)	[illegible]2.97	-5.16	+0.34

OPT1: VNCL4040, OPT2: VCNL36825T, * change in setup

IV. Results and Discussion

A. Dew Sensor Characterization

The capacitive sensor was measured to have a capacitance of 180 [illegible] at ambient temperature and humidity. It is charged and discharged through $1\,\mathrm{M\Omega}$ resistors, the sampling frequency for the inverter circuitry is $170\,\mathrm{MHz}$ and its thresholds $1.05\,\mathrm{V}$ and 1.[illegible] V. This results in a period of $T_{RC} = 115.34\,\mathrm{\mu s}$ or a frequency of $8.67\,\mathrm{kHz}$ using following equation [9]:

$$T = RC \cdot \ln\left[\frac{(V_{DD} - V_{th,n})V_{th,p}}{(V_{DD} - V_{th,p})V_{th,n}}\right]. \tag{1}$$

With a sampling period of $T_s = \frac{1}{170\,\mathrm{MHz}} = 5.88\,\mathrm{ns}$, this results in a sensitivity of 5[illegible] pm, which is severely limited however by noise introduced into the measurement system such as fluctuations in supply and threshold voltage, fluctuations in sampling frequency, electromagnetic interference, temperature and mechanical forces. For noise estimation, the capacitive sensor was placed in a quasi-static environment according to external sensors (ΔT = 20 mK, ΔRH = 0.3 %) for a duration of 30 s, resulting in a signal-to-noise ratio (SNR) of 81.2 dB.

The optical sensors are specified to detect objects within a range of 0 mm to [illegible]0 mm, yet their output code at a given distance is different as to their different emitting power and angle. Both sensors yield 16 bit output codes which correlate to the amount of dew collected on the reflective surface. In the same test setup for noise estimation, the sensors yield optical readings with SNRs of 70.3 dB and 71.3 dB respectively.

B. Initial Measurements

The first test consisted of reading initial sensor measurements for the respective temperatures and humidities. The capacitive measurement is highly influenced by the humidity, as can be seen in fig. 2. Lower relative humidities result in less capacitance and thus an increased switching frequency of the relaxation oscillator, whereas the temperature has no clear influence on the measurements for a fixed relative humidity. The optical measurements do not exhibit significant dependence on relative or absolute humidity.

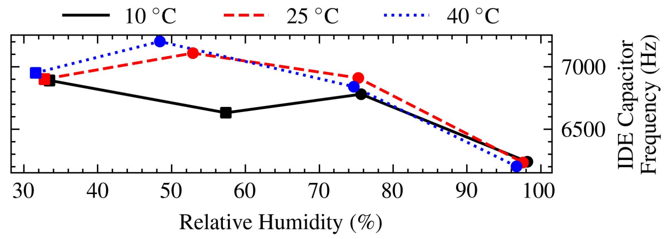

Fig. 2: Initial frequencies for the different measurements. Rectangular markers show the results after test setup changes.

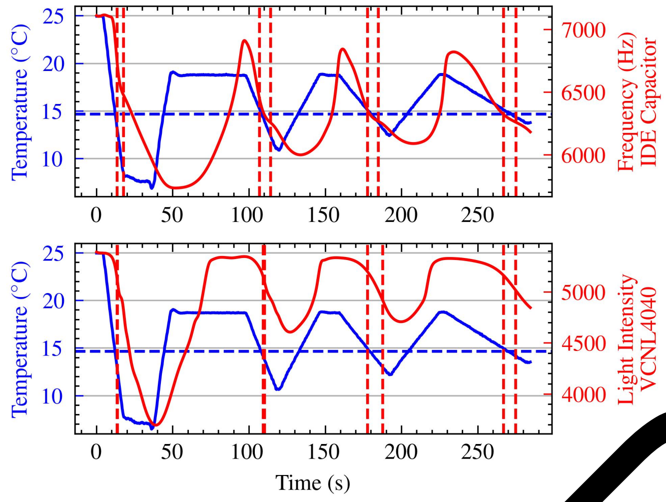

Fig. 3: Measurement of the dew point temperature for T = 25.0 °C, RH = 52.89 %. The horizontal dashed lines indicate the actual dew point temperature, the vertical dashed lines indicate the determined dew point temperature range in each cooldown cycle ($-1.3\,\frac{\mathrm{K}}{\mathrm{s}}$, $-0.4\,\frac{\mathrm{K}}{\mathrm{s}}$, $-0.2\,\frac{\mathrm{K}}{\mathrm{s}}$ and $-0.[illegible]\,\frac{\mathrm{K}}{\mathrm{s}}$).

C. Dew Point Detection

Figure 3 shows the dew point measurement of the IDE capacitor and VCNL4040 in the test configuration of T = 25.0 °C and RH = 52.89 %. The measurement diagram of VCNL36825T is not shown due to space constraints, but resembles that of the VCNL4040.

The first cooldown cycle is used for fast working dew point range detection, limiting the following cycles to only a few degrees celsius. The curves of the capacitive and optical sensors differ significantly throughout the measurement and hence require different analysis methods in order to determine the dew point temperature. The capacitive element is very sensitive even to smallest changes in temperature. As suggested by the results of the initial measurements, this may be caused by induced local changes of relative humidity. The dew point is marked by a small step in the frequency slope, hence it is determined to be within the timestamps of the maximum of the second derivative and the maximum of the first derivative. The frequency around the dew point differs significantly depending on the ambient temperature and humidity conditions.

Contrastingly, the output signal of the proximity sensors is much more stable until close to the dew point. As expected, right around the timepoint of condensation, there is a significant change in light intensity due to refraction and absorption caused by the water molecules. The dew point is found to be always within the minimum of the second derivative and the minimum of the first derivative.

Due to the limited amount of test data, no interpolation techniques have been employed for improving the accuracy of the determined dew point temperature. Instead, the on average closest fitting temperature values of the last cycles have been chosen, that is for the capacitive sensor the start and for the optical sensors the end of the determined range. The resulting relative humidity errors for each sensor and measurement are shown in table I. Figure 4 shows the error range and the mean error over all measurements for each sensor. The error range of the measured dew point temperature is found to be around 1.2 °C and 1.8 °C for the VCNL4040 and IDE capacitor respectively. This value is one order of magnitude higher than the accuracy of the used temperature sensor, indicating the dew point detection to be the limiting factor. A further decrease of cooldown speed for a higher resolution is unlikely to yield substantially higher accuracy, as the improvement compared to the previous cooldown cycle is already insignificant. Taking the large error range of around [illegible].5 °C of the VCNL36825T into consideration, it is suggested that error detection schemes based on the found temperature range and a data-driven interpolation of the dew point within said range may need to be employed. Repeated measurements with real-time dew point analysis have the potential to ensure a sufficiently precise result.

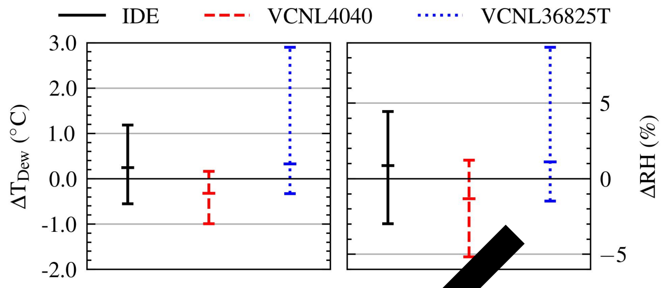

Fig. 4: Average, minimum and maximum measured dew point temperature and relative humidity deviation for each sensor.

V. Conclusion

The sensor platform employs the optical and capacitive dew point sensing in parallel and yields a comprehensive comparison of the underlying differences in readout. In the realized setup, there is no clear winner between the two principles, as both require careful interpretation of the acquired data to determine the exact timepoints of condensation. Using simple data analysis methods, the dew point could be determined with a deviation of less than 1 °C. For higher accuracies, the use of more sophisticated data analysis methods and a real-time error estimation is suggested.

References

[1] G. Korotcenkov, *Handbook of Humidity Measurement, Volume 2: Electronic and Electrical Humidity Sensors*. Boca Raton: CRC Press, Feb. 2019, ISBN: 978-0-203-73188-8. DOI: 10.1201/b22370.

[2] Z. Chen and C. Lu, "Humidity Sensors: A Review of Materials and Mechanisms," *Sensor Letters*, vol. 3, no. 4, pp. 274–295, Dec. 2005. DOI: 10.1166/sl.2005.045.

[3] R. Srivastava, "Humidity Sensor: An Overview," *International Journal of Green Nanotechnology*, vol. 4, no. 3, pp. 302–309, Jul. 2012, ISSN: 1943-0892. DOI: 10.1080/19430892.2012.706001.

[4] J. Nie, J. Liu, and X. Meng, "A new type of fast dew point sensor using quartz crystal without frequency measurement," *Sensors and Actuators B: Chemical*, vol. 236, pp. 749–758, Nov. 2016, ISSN: 0925-4005. DOI: 10.1016/j.snb.2016.06.034.

[5] J. Tao, Y. Luo, L. Wang, *et al.*, "An ultrahigh-accuracy Miniature Dew Point Sensor based on an Integrated Photonics Platform," *Scientific Reports*, vol. 6, no. 1, p. 29 672, Jul. 2016, ISSN: 2045-2322. DOI: 10.1038/srep29672.

[6] *Scipy.interpolate.splrep — SciPy v1.12.0 Manual*, https://docs.scipy.org/doc/scipy/reference/generated/scipy.interpolate.splrep.html.

[7] P. Dierckx, "An algorithm for smoothing, differentiation and integration of experimental data using spline functions," *Journal of Computational and Applied Mathematics*, vol. 1, no. 3, pp. 165–184, Sep. 1975, ISSN: [illegible]77-0427. DOI: 10.1016/0771-050X(75)9003[illegible].

[8] L. Greenspan, "Humidity Fixed Points of Binary Saturated Aqueous Solutions," *Journal of Research of the National Bureau of Standards. Section A, Physics and Chemistry*, vol. 81A, no. 1, pp. 89–96, [illegible], ISSN: 0022-4332. DOI: 10.6028/jres.0[illegible].

[9] Texas Instruments, "Relaxation Oscillator Circuit," Jun. 2018.